Intramolecular Charge Transfer Controls Switching Between Room Temperature Phosphorescence and Thermally Activated Delayed Fluorescence**

Chengjian Chen,[†] Rongjuan Huang,[†] Andrei S. Batsanov, Piotr Pander, Yu-Ting Hsu, Zhenguo Chi, Fernando B. Dias, and Martin R. Bryce*

Abstract: Chemical modification of phenothiazine–benzophenone derivatives tunes the emission behavior from triplet states by selecting the geometry of the intramolecular charge transfer (ICT) state. A fundamental principle of planar ICT (PICT) and twisted ICT (TICT) is demonstrated to obtain selectively either room temperature phosphorescence (RTP) or thermally activated delayed fluorescence (TADF), respectively. Time-resolved spectroscopy and time-dependent density functional theory (TD-DFT) investigations on polymorphic single crystals demonstrate the roles of PICT and TICT states in the underlying photophysics. This has resulted in a RTP molecule **OPM**, where the triplet states contribute with 89% of the luminescence, and an isomeric TADF molecule **OMP**, where the triplet states contribute with 95% of the luminescence.

Organic luminescent materials based on donor–acceptor ICT emitters (D–A or D–A–D) can efficiently harvest triplet excited states. For non-planar donors quantum chemistry calculations suggest that the D–A bridges should have optimal geometries to facilitate different ICT processes.[1] For example, different conformers of the D unit can show markedly different triplet harvesting efficiencies. To promote the most efficient conformer for TADF or RTP is a challenge.[1f,g]

TADF and RTP materials are of great interest due to their potential applications in optoelectronic and biological areas.[2] Phosphorescent materials can achieve up to 100% internal quantum efficiency (IQE) by utilizing singlet-to-triplet intersystem crossing (ISC). Fast ISC is usually promoted by incorporating a heavy atom or an ICT state into the molecular structure to facilitate strong spin-orbit coupling (SOC).[3] Metal-free phosphors are relatively rare and generally suffer from extremely weak phosphorescence under ambient conditions due to the spin forbidden nature of the triplet to singlet transition.[2-4] Therefore, to achieve pure organic RTP, the SOC strength needs to be enhanced, and the nonradiative dissipations should be suppressed. Mixing the singlet-triplet energies of different molecular orbitals (El-Sayed's rule) by incorporating, for example, aromatic carbonyls and ICT interactions, can promote strong SOC and hence efficient ISC for RTP.[2c,4,5]

Another way to obtain 100% IQE, without heavy metals, is TADF, which is based on converting triplet states to fluorescent singlet states by thermally activated reverse ISC (RISC).[1c] To increase the RISC rate necessitates maximizing the SOC and simultaneously minimizing the exchange energy gap between the lowest singlet and triplet states, $\Delta E(S_1,T_1)$. Indeed, minimizing the energy gaps between charge-transfer (CT) and local-excited (LE) triplet states, including ^{3}LE-^{3}CT and ^{3}LE-^{1}CT, is critical for efficient TADF, since hyperfine coupling between ^{1}CT and ^{3}CT is usually inactive.[6] Recently, three regimes for TADF were identified for a D–A–D emitter by changing the polarity of the host environment.[6a] This arises because ICT states often differ markedly in their electronic structure and molecular geometry, and are thus very sensitive to the molecules' environment. Accordingly, a strategy that can stabilize molecular geometry with the desirable nearly-perpendicular D–A units in the TICT state is important. Enforcing rigidity on D–A molecules by chemical functionalization is exploited in new ways in the present work.[7]

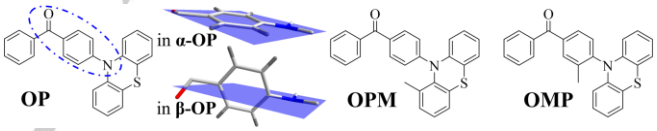

Figure 1. Structures of **OP**, **OPM** and **OMP** studied in this work

The quasi-axial (ax) and quasi-equatorial (eq) conformers of phenothiazine derivatives were computationally predicted in 2001.[1f,8] Recently, the two conformers were shown experimentally to co-exist in a D_{ax}–A–D_{eq} molecule.[9] We now report three D–A phenothiazine–benzophenone derivatives (**OP**, **OPM**, and **OMP**, Figure 1 and Scheme S1) wherein carbonyl units can provide orbitals to promote ISC from S_1 to T_n states.[2c,4] **OPM** and **OMP** have a methyl substituent on the D and A unit, respectively, to provide steric constraints.[10] Since the ax and eq conformers of phenothiazine derivatives have not previously been separated,[8,9,10a] we applied two very different conditions to grow single crystals of **OP**, i.e. a dilute solution with slow evaporation, and a saturated solution without evaporation. The ax and eq phenothiazine conformers were exclusively obtained in the single crystals, **α-OP** and **β-OP**, respectively. Figures 2A and S1 (in Supporting Information) show the X-ray molecular structures of **α-OP** and **β-OP**.

[*] Dr. C. Chen, Dr. A. S. Batsanov, Dr. Y.-T. Hsu, Prof. M. R. Bryce
Department of Chemistry, Durham University, Durham, DH1 3LE, UK. E-mail: m.r.bryce@durham.ac.uk
R. Huang, P. Pander, Dr. F. B. Dias
Department of Physics, Durham University, Durham, DH1 3LE, UK.
Dr. C. Chen, Prof. Z. Chi
PCFM Lab, GD HPPC Lab, School of Chemistry, Sun Yat-sen University, Guangzhou 510275, P. R. China
[†] Dr. C. Chen and R. Huang contributed equally.
[**] This work was financially supported by EPSRC grant number grant number EP/L02621X/1. The authors thank Prof. A. Beeby, Prof. S. J. Clark and Dr. J. S. Ward for helpful discussions.
Supporting information can be found via a link at the end.

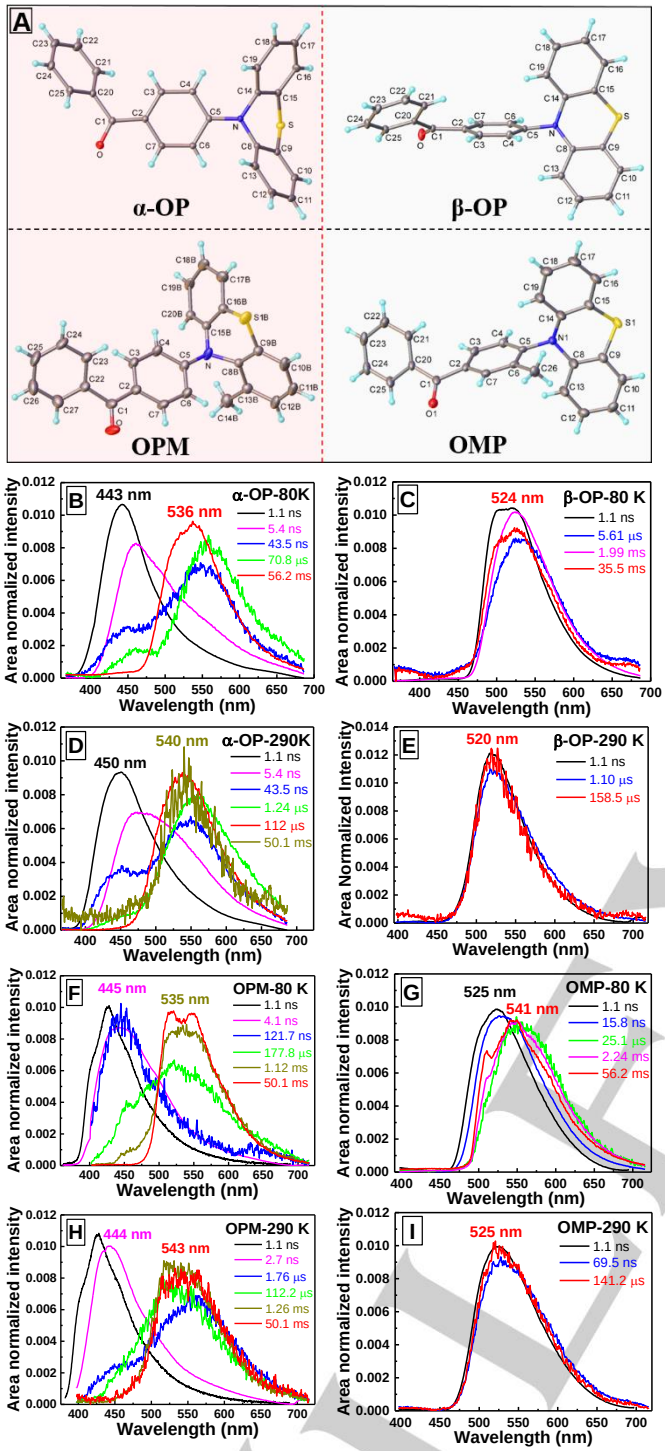

Figure 2. X-ray molecular structures of **α-OP**, **β-OP**, **OPM**, and **OMP**(**α-OMP**) (A). Time resolved area normalized emission spectra of crystals: **α-OP** at 80 K (B), 290 K (D), **β-OP** at 80 K (C), 290 K (E), **OPM** at 80 K (F), 290 K (H), and **OMP**(**α-OMP**) at 80 K (G), 290 K (I). All spectra were excited at 355 nm.

In the ax **α-OP** the three N–C bonds are almost coplanar with the benzene ring of the benzophenone. In the eq **β-OP** the corresponding geometry is nearly perpendicular (Figures 1A and S1). A mutually perpendicular D–A geometry is required for the typical TICT model, whereas, in the PICT model, a relatively small energy gap $\Delta E(S_1,S_2)$ plays a more critical role in the ICT process, rather than the coplanarity of the D–A moieties.[11a] The $\Delta E(S_1,S_2)$ of **α-OP** was calculated to be 0.09 eV (Figure 3) which is a negligible gap that favours the vibronic coupling between S_1 and S_2 states. Figure S4 shows that **α-OP** and **β-OP** have almost equal stable energies; thus any attempt to explain results based on one selected conformation in solution or matrix is unsatisfactory.[8b]

4-(*N*,*N*-dimethylamino)benzonitrile (DMABN) and its derivatives have been widely studied to elucidate the roles of different ICT states.[11a] According to their design principles, a methyl group was introduced at specific positions of **OP**, i.e. molecules **OPM** and **OMP**, to rigidify the conformers and stabilize PICT and TICT states, respectively. Two similar ax conformers were observed in the single crystals of **OPM**. Three different polymorphs of **OMP** (**α**, **β** and **γ**) were obtained: all three show similar eq conformers (Figures 2A and S7).

To investigate the PICT and TICT states, time-resolved spectroscopy was employed from 80 K to 290 K to measure luminescence from crystals (Figures 2B-I). In Figures 2B and 2D, the dual emission of **α-OP** was identified as the LE and CT processes in accordance with the PICT model.[11] The spectra had the profile and dynamic behavior of a CT band undergoing a transient Stokes shift.[12] Since dual emission is very common in the PICT model, **α-OP** emits blue at ~450 nm and yellow at ~540 nm, which provides a design for white light emission from a single organic molecule.[2b,8c,13] The white emission from **OPM** crystals (Figure S2) demonstrates this application of the PICT model.

α-OP shows dual emission on the microsecond time-scale (up to 70.8 μs, Figure 2B, and 1.24 μs Figure 2D), giving clear indication of the RISC from triplet to singlet states. Moreover, **α-OP** shows phosphorescence at ~540 nm at 290 K, and at ~536 nm at 80 K. Time dependent density functional theory (TD-DFT) calculations (see below) show that the **α-OP** geometry favors the n-π* transition of the carbonyl group and hence facilitates ISC according to El-Sayed's rule.[4,5] Meanwhile, the hybrid n-π* and π-π* orbital configurations in **α-OP** activate a radiative transition from T_1 to S_0 leading to phosphorescence after being rigidified in the crystalline state.

Figures 2F and 2H show that for **OPM** the blue emission at ~445 nm has LE character with well-resolved spectra at both 80 K and 290 K. Well-resolved LE emission is generally observed only under frozen conditions (e.g. 80 K) or in a restricted structure. The 290 K data imply that the methyl group in **OPM** locks the conformation into the PICT geometry, which simultaneously minimizes non-radiative deactivation processes of triplet excitons. **OPM** shows obvious RTP (Figure 2H). To further enhance the rigidity, two methyl groups were attached to the phenothiazine to give **OP2M** (Figure S3). LE emission is observed in **OP2M** in both toluene solution and Zeonex film compared to **OPM** (Figures S6 and S17).

In contrast to **OPM**, both **β-OP** and **OMP** show perfect TADF spectra, i.e. the delayed and prompt spectra are identical (Figures 2E and 2I). The **OMP** phosphorescence (from ^{3}LE) is at ~541 nm at 2.24 ms and 56.2 ms (Figure 2G), and is crucial for efficient TADF in the vibronic coupling RISC model.[6] Both **β-OMP** and **γ-OMP** (Figure S7) show the eq conformers, thus TADF properties were obtained (Figures S13 and S14).

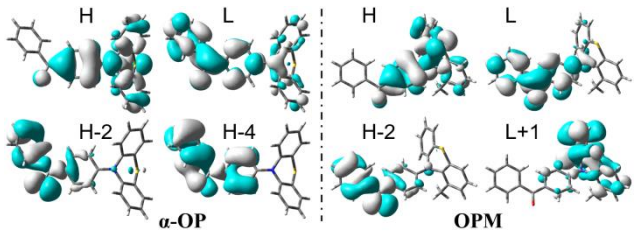

	State	Transition configuration
α-OP	S_1/3.60 eV	H-4→L 7.7%, H-2→L 76.1%, H→L 7.9%.
	S_2/3.69 eV	H-2→L 7.9%, H→L 84.8%.
	T_1/2.80 eV	H-2→L 5.4%, H→L 75.7%.
	T_2/3.09 eV	H-4→L 2.9%, H-2→L 79.4%, H→L 5.8%.
OPM	S_1/3.60 eV	H-2→L 76.7%, H→L 8.5%.
	S_2/3.74 eV	H-2→L 7.3%, H→L 68.6%, H→L+1 21.1%.
	T_1/2.86 eV	H-2→L 15.8%, H-1→L 11.7%, H→L 59.3%.
	T_2/3.15 eV	H-2→L, 72.3%, H→L, 14.2%.

Figure 3. Frontier molecular orbitals of **α-OP** and **OPM**, and electronic transitions at B3LYP/6-31G* (H = HOMO; L = LUMO). The same components of S_1 are in red text.

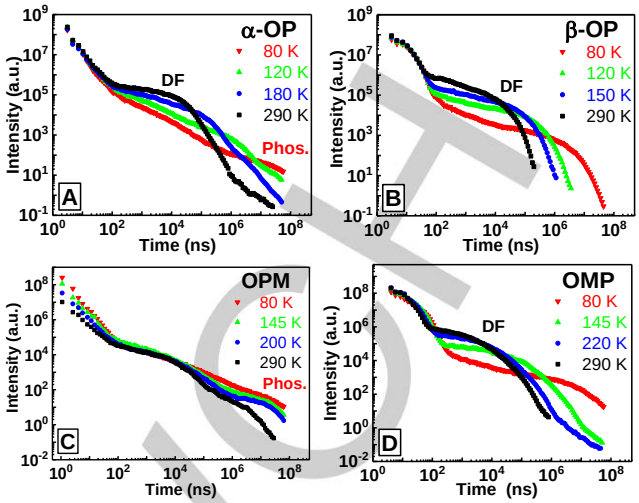

Figure 4. Temperature dependence of emission decays of **α-OP** (A), **β-OP** (B), **OPM** (C) and **OMP**(**α-OMP**) (D) crystals from 290 K to 80 K.

To probe the mechanism underlying the observed spectra, TD-DFT investigations were performed on the singlet and triplet excited states.[2a,14] The frontier molecular orbitals (H = highest occupied molecular orbital, HOMO; L = lowest unoccupied molecular orbital, LUMO) and electronic transitions are shown in Figures 3, S8-S10 and Tables S3-S7 using B3LYP/6-31G*. Similar orbital distributions were obtained using M062X/6-31G* and B3LYP/6-31G* functionals (Figures S11 and S12). S_1, S_2, T_1 and T_2 of **α-OP** and **OPM** are mixed electronic states with n-π* (H-2→L) and π-π* (H→L) transitions, which involve the oxygen lone pairs (carbonyl group) and the conjugated structure, respectively (Figure 3).[2b] Meanwhile, S_1 and T_2 are dominated by an n-π* transition, while S_2 and T_1 possess more π-π* transition character. Therefore, SOC occurs from ^{1}(n-π*) to ^{3}(π-π*), and from ^{1}(π-π*) to ^{3}(n-π*) because of effective orbital overlap according to El-Sayed's rule.[2c] In addition, S_1, S_2, T_1 and T_2 are hybridized local and charge-transfer (HLCT) states, since H-2→L is assigned as an LE transition and H→L is assigned as a CT transition.[15] According to reported HLCT molecules, RISC from upper triplet to singlet levels probably occurs in **α-OP** and **OPM** as $\Delta E(S_1,T_1)$ is large (0.80 eV for **α-OP** and 0.74 eV for **OPM**).[15] Interestingly, the ^{3}LE emission (2.24 and 56.2 ms, Figure 2G) of **OMP** is ascribed to the contributions from the phenothiazine group (Figure S15), according to the calculated triplet states which show a H→L+1 transition (Table S4 and Figure S9). Furthermore, both S_1 and T_1 show CT transitions (H→L), thus, the efficient RISC model of ^{3}CT-^{3}LE-^{1}CT is demonstrated by **OMP**(**α-OMP**) with a small $\Delta E(S_1,T_1)$ of 0.03 eV (Table S5).[6a]

The time-resolved temperature dependence of the emission decays were plotted from 290 K to 80 K (Figure 4). **α-OP** at 80 K has three components, ascribed to prompt fluorescence (PF), delayed fluorescence (DF) and phosphorescence (Phos.) based on their different temperature effects (Figure 4A).[15]

Since the methyl substituent in **OPM** suppresses non-radiative pathways by rigidifying the structure, triplet excitons are stabilized. Consequently, Figure 4C shows a gradual decay of phosphorescence and reveals RTP.[4] Accordingly, we propose that hybridizing n-π* and π-π* transitions in the triplet states of **α-OP** and **OPM** is the key to activating phosphorescence.[2c] Since **α-OP** and **OPM** are PICT systems, with two singlet states (S_1 and S_2) that are close in energy, and with different transition characters to enhance ISC, we propose the PICT model is a new design strategy for RTP after rigidifying the geometry.[7,11] Figure 4B shows a gradual DF decay component of **β-OP** with a very sensitive temperature response, i.e. this TICT molecule presents efficient TADF with a small $\Delta E(S_1,T_1)$ of 0.05 eV (Table S4). Analogously, **OMP**(**α-OMP**) and **β-OMP** have similar geometries to **β-OP** and their efficient TADF properties are seen in Figures 4D and S13. Interestingly, **γ-OMP** retains nearly perpendicular geometry, despite showing a different conformer (Figure S7). Therefore, **γ-OMP** has a very sensitive temperature response in the DF decay component (Figure S14C). Consequently, the TICT model is strictly controlled with the methyl group, and hence the TADF properties are effectively retained. To further elucidate the development of triplet states, the steady state emission of the molecules in Zeonex matrix was measured in vacuum and in air at RT. Figures S17B and S17C show that the triplet states contribute 89% and 95% of the **OPM** and **OMP** luminescence, respectively.[8c] To further investigate the PICT and TICT models, organic light emitting diodes (OLEDs) were fabricated using **OPM** and **OMP** as the emitters (Figure S18 and Table S8). Device 1 based on **OMP** had an emission peak at 558 nm with a maximum external quantum efficiency (EQE) of 10.2%, which was attributed to a TADF mechanism. As expected, dual emission was observed from Device 2, involving **OPM** and RTP with a maximum EQE of only 0.6%.

In summary, the ax and eq conformers **α-OP** and **β-OP** are ideal PICT and TICT model systems, respectively. Based on TD-DFT calculations and photoluminescence spectra the PICT

model is proposed as a new strategy for obtaining RTP. We have established that selectively attaching a methyl group to the **OP** molecule can stabilize either the PICT geometry in **OPM**, or the TICT geometry in the isomer **OMP**. White light emission from **OPM** is a result of dual emissive processes according to the PICT mechanism. This rational conformational control has led to efficient utilization of triplet states for RTP in **OPM** and for TADF in **OMP**. Related luminescent D–A molecules can be developed using these guidelines.

Keywords: room termperature phosphorescence • thermally activated delayed fluorescence • charge transfer • donor–acceptor systems • polymorphism

[1] a) M. Kasha, H. R. Rawls, *Photochem. Photobiol.* **1968**, *7*, 561–569; b) D. Di, A. S. Romanov, L. Yang, J. M. Richter, J. P. H. Rivett, S. Jones, T. H. Thomas, M. Abdi Jalebi, R. H. Friend, M. Linnolahti, M. Bochmann, D. Credgington, *Science* **2017**, *356*, 159–163; c) Y. Liu, C. Li, Z. Ren, S. Yan, M. R. Bryce, *Nat. Rev. Mater.* **2018**, *3*, 18020; d) X-K. Chen, Y. Tsuchiya, Y. Ishikawa, C. Zhong, C. Adachi, J-L. Brédas, *Adv. Mater.* **2017**, 1702767; e) Y-Z. Shi, K. Wang, X. Li, G-L. Dai, W. Liu, K. Ke, M. Zhang, S-L. Tao, C-J. Zheng, X-M. Ou, X-H. Zhang, *Angew. Chem. Int. Ed.* **2018**, *57*, 9480–9484; *Angew. Chem.* **2018**, *130*, 9624–9628; f) K. Wang, C-J. Zheng, W. Liu, K. Liang, Y-Z. Shi, S-L. Tao, C-S. Lee, X-M. Ou, X-H. Zhang, *Adv. Mater.* **2017**, *29*, 1701476; g) R. Huang, J. S. Ward, N. A. Kukhta, J. Avo, J. Gibson, T. Penfold, J. C. Lima, A. S. Batsanov, M. N. Berberan-Santos, M. R. Bryce, F. B. Dias, *J. Mater. Chem. C* **2018**, *6*, 9238–9247.

[2] a) Z. An, C. Zheng, Y. Tao, R. Chen, H. Shi, T. Chen, Z. Wang, H. Li, R. Deng, X. Liu, W. Huang, *Nat. Mater.* **2015**, *14*, 685–690; b) Z. He, W. Zhao, J. W. Y. Lam, Q. Peng, H. Ma, G. Liang, Z. Shuai, B. Z. Tang, *Nat. Commun.* **2017**, *8*, 416; c) W. Zhao, Z. He, J. W. Y. Lam, Q. Peng, H. Ma, Z. Shuai, G. Bai, J. Hao, B. Z. Tang, *Chem* **2016**, *1*, 592–602.

[3] D. Chaudhuri, E. Sigmund, A. Meyer, L. Röck, P. Klemm, S. Lautenschlager, A. Schmid, S. R. Yost, T. Van Voorhis, S. Bange, S. Höger, J. M. Lupton, *Angew. Chem. Int. Ed.* **2013**, *52*, 13449–13452; *Angew. Chem.* **2013**, *125*, 13691–13694.

[4] O. Bolton, K. Lee, H-J. Kim, K. Y. Lin, J. Kim, *Nat. Chem.* **2011**, *3*, 205–210.

[5] M. A. El-Sayed, *J. Chem. Phys.* **1963**, *38*, 2834–2838.

[6] a) M. K. Etherington, J. Gibson, H. F. Higginbotham, T. J. Penfold, A. P. Monkman, *Nat. Commun.* **2016**, *7*, 13680; b) P. K. Samanta, D. Kim, V. Coropceanu, J-L. Brédas, *J. Am. Chem. Soc.* **2017**, *139*, 4042–4051; c) T. Matulaitis, P. Imbrasas, N. A. Kukhta, P. Baronas, T. Bučiūnas, D. Banevičius, K. Kazlauskas, J. V. Gražulevičius, S. Juršėnas, *J. Phys. Chem. C* **2017**, *121*, 23618–23625; d) T. Ogiwara, Y. Wakikawa, T. Ikoma, *J. Phys. Chem. A* **2015**, *119*, 3415–3418.

[7] a) Z. R. Grabowski, K. Rotkiewicz, *Chem. Rev.* **2003**, *103*, 3899−4031; b) Z. Zhang, C-L. Chen, Y-A. Chen, Y-C. Wei, J. Su, H. Tian, P-T. Chou, *Angew. Chem. Int. Ed.* **2018**, 57, 9880–9884; *Angew. Chem.* **2018**, *130*, 10028–10032.

[8] a) J. Daub, R. Engl, J. Kurzawa, S. E. Miller, S. Schneider, A. Stockmann, M. R. Wasielewski, *J. Phys. Chem. A* **2001**, 105, 5655–5665; b) A. Stockmann, J. Kurzawa, N. Fritz, N. Acar, S. Schneider, J. Daub, R. Engl, T. Clark, *J. Phys. Chem. A* **2002**, 106, 7958−7970; c) Z. Xie, C. Chen, S. Xu, J. Li, Y. Zhang, S. Liu, J. Xu, Z. Chi, *Angew. Chem. Int. Ed.* **2015**, *54*, 7181–7184; *Angew. Chem.* **2015**, *127*, 7287–7290; d) J. Yang, J. Qin, P. Geng, J. Wang, M. Fang, Z. Li, *Angew. Chem. Int. Ed.* **2018**, *57*, 14174–14178; *Angew. Chem.* **2018**, *130*, 14370–14374.

[9] a) M. K. Etherington, F. Franchello, J. Gibson, T. Northey, J. Santos, J. S. Ward, H. F. Higginbotham, P. Data, A. Kurowska, P. L. Dos Santos, D. R. Graves, A. S. Batsanov, F. B. Dias, M. R. Bryce, T. J. Penfold, A. P. Monkman, *Nat. Commun.* **2017**, *8*, 14987; b) B. Xu, Y. Mu, Z. Mao, Z. Xie, H. Wu, Y. Zhang, C. Jin, Z. Chi, S. Liu, J. Xu, Y-C. Wu, P-Y. Lu, A. Lien, M. R. Bryce, *Chem. Sci.* **2016**, *7*, 2201–2206; c) M. Okazaki, Y. Takeda, P. Data, P. Pander, H. Higginbotham, A. P. Monkman, S. Minakata, *Chem. Sci.* **2017**, *8*, 2677–2686.

[10] a) N. Aizawa, C-J. Tsou, I. S. Park, T. Yasuda, *Polym. J.* **2017**, *49*, 197–202; b) L-S. Cui, H. Nomura, Y. Geng, J. U. Kim, H. Nakanotani, C. Adachi, *Angew. Chem. Int. Ed.* **2017**, *56*, 1571–1575; *Angew. Chem.* **2017**, *129*, 1593–1597; c) J. S. Ward, R. S. Nobuyasu, A. S. Batsanov, P. Data, A. P. Monkman, F. B. Dias, M. R. Bryce, *Chem. Commun.* **2016**, *52*, 2612–2615.

[11] a) S. I. Druzhinin, P. Mayer, D. Stalke, R. Bülow, M. Noltemeyer, K. A. Zachariasse, *J. Am. Chem. Soc.* **2010**, *132*, 7730–7744; b) H. Naito, K. Nishino, Y. Morisaki, K. Tanaka, Y. Chujo, *Angew. Chem. Int. Ed.* **2017**, *56*, 254–259; *Angew. Chem.* **2017**, *129*, 260–265.

[12] N. Mataga, T. Okada and H. Masuhara, Dynamics and Mechanisms of Photoinduced Electron Transfer and Related Phenomena; Elsevier: Amsterdam, **1992**.

[13] Z. Xie, Q. Huang, T. Yu, L. Wang, Z. Mao, W. Li, Z. Yang, Y. Zhang, S. Liu, J. Xu, Z. Chi, M. P. Aldred, *Adv. Funct. Mater.* **2017**, *27*, 1703918.

[14] M. J. Frisch, et al., Gaussian 09 (Revision D.01), Gaussian Inc., Wallingford CT, **2009**.

[15] a) L. Yao, S. Zhang, R. Wang, W. Li, F. Shen, B. Yang, Y. Ma, *Angew. Chem. Int. Ed.* **2014**, *53*, 2119–2123; *Angew. Chem.* **2014**, *126*, 2151–2155; b) D. Hu, L. Yao, B. Yang, Y. Ma, *Phil. Trans. R. Soc. A* **2015**, *373*: 20140318.

[16] T. Ogiwara, Y. Wakikawa, T. Ikoma, *J. Phys. Chem. A* **2015**, *119*, 3415–3418.

[17] CCDC 1495259, 1495260, 1495261, 1496581, 1496582, 1817433 and 1817434 contain the supplementary crystallographic data for this paper. These data are available free of charge from the Cambridge Crystallographic Data Centre.

COMMUNICATION

Intramolecular Charge Transfer Controls Switching Between Room Temperature Phosphorescence and Thermally Activated Delayed Fluorescence: Rapid and efficient utilization of triplet states to generate room temperature phosphorescence (RTP) or highly efficient thermally activated delayed fluorescence (TADF) is achieved by structural modification to give a planar or twisted intramolecular charge transfer (PICT or TICT) geometry, respectively.

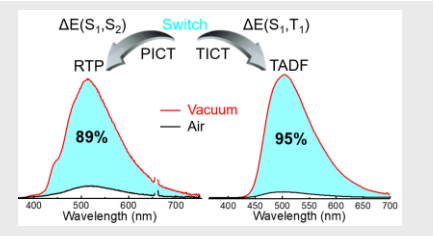

*Chengjian Chen,† Rongjuan Huang,† Andrei S. Batsanov, Piotr Pander, Yu-Ting Hsu, Zhenguo Chi, Fernando B. Dias, and Martin R. Bryce**

Page No. – Page No.

Intramolecular Charge Transfer Controls Switching Between Room Temperature Phosphorescence and Thermally Activated Delayed Fluorescence